


Remote Sensing of Spatial and Temporal Mapping of Flare Impacts in the Niger Delta, Nigeria

 Barnabas O. Morakinyo*

Department of Surveying & Geoinformatics, Faculty of Environmental Sciences, BAZE University, Abuja, Nigeria

Received October 15, 2024; Accepted March 6, 2025

Abstract: This research focuses on the mapping of spatial and temporal effects of flare on vegetation cover. The data (11 Landsat 5 TM, 49 Landsat 7 ETM+, 27 Landsat 8 OLI-TIRS, and 15 Landsat 9 OLI-TIRS) dated from 10/10/1984 to 17/12/2023 with < 3 % cloud cover was used to study 11 flaring sites in the Niger Delta. Data processing and analysis were carried out using MATLAB codes. Normalized Difference Vegetation Index (NDVI) for Landsat 5 and 7 bands (1-4) and Landsat 8 and 9 bands (2-5) was determined from the atmospherically corrected multispectral bands. The results show that the temporal in NDVI is specific to each site, and that the effect of the flares on the vegetation cover does not majorly depend on the size of facility. Eleme I (-2.71×10^{-5} - 2.32×10^{-5}) and II (-1.740×10^{-4} - 2.074×10^{-5}) presented significant results for a small portion of the area. Umuruolu (-1.679×10^{-5} - 5.868×10^{-5}) and Bonny (-3.089×10^{-5} - 2.423×10^{-5}) show significant results for a wider area which could be because of the number of flare stacks within them 4 and 5 respectively. All small and medium facilities show statistically significant results which could be attributed to the rate and volume of gas burning from them. Therefore, it can be concluded that Landsat data can be used to map the spatial and temporal impacts of flare on vegetation cover in the Niger Delta.

Keywords: *Remote Sensing, Environmental Science, Thematic Mapping, Land Cover, Environmental Studies.*

Introduction

The Niger Delta region is in the Southern part of Nigeria; and it consists of Akwa Ibom, Bayelsa, Cross River, Delta and Edo states from South South region; Abia and Imo states from South East region; and Ondo State from South West region (Morakinyo, 2015; Onosode, 2003). The Niger Delta is an arcuate shaped basin that consists of diverse vegetation and four different ecological zones such as coastal ridge barriers, brackish/freshwater swamp forests, mangrove forests and lowland rain forests (Odukoya, 2006).

The Niger Delta is the home for oil and gas exploration, exploitation and processing activities in Nigeria. Hence, activities of multinational oil companies such as Shell Petroleum Company, AGIP, Total, ELF, etc. are ongoing. The effects of oil and gas activities in the environment of the Niger Delta includes increase in temperature (Lu et al., 2020; Morakinyo et al., 2019); environmental pollution (Morakinyo et al., 2023a; Morakinyo et al., 2023b; Ubugala & Morakinyo, 2023; Lu et al., 2020); contamination of vegetation (Morakinyo, 2015); destruction of vegetation and agricultural pursuits (Morakinyo et al., 2020a,b; Nwaogu & Onyeze, 2020), stunted growth and or death of farm produce, reduction and destruction of agricultural activities and vegetation (Musa et al., 2024; Morakinyo et al., 2023a; Morakinyo, 2023c; Morakinyo et al., 2021; Morakinyo et al., 2020 a, b).

Remote sensing technology deals with the mapping of the environment using space borne platforms (Jansen & Gregorio, 2004). It is essential in the production of large, repetitive geospatial data of the environment. The geospatial information acquired at different locations can be employed for the characterization and assessment of changes in the environment (Yuan et al., 2005). Characteristics of remotely sensed data are spatial, temporal, and spectral and are used for mapping of land cover dynamics, land use land cover (LULC) changes, retrieval of land surface temperature (LST) (Morakinyo et al., 2022), planning etc. for decision making purposes (Berlanga-Robles and Ruiz-Luna 2002). The availability of satellite data has made it possible to observe LC from space (Mollicone et al.

*Corresponding: E-Mail: barnabas.ojo@bazeuniversity.edu.ng, Tel: +234(0)8103676990

2003); and geospatial information needed for evaluation of changes on Earth's surface are collected at different time intervals (Jensen 2005).

Landsat data has been useful in the study of the environment in several ways such as assessment of LULC (Jensen 2005); monitoring of vegetation health (Morakinyo *et al.*, 2023a); LST retrieval (Lu *et al.*, 2020); forest and agricultural areas monitoring (Campbell 2007); urbanization and planning processes (Jensen & Cowen 1999); urban studies (Wang *et al.* 2020). Open access to satellite data enables spatially valid datasets over large areas with great spatial information and temporal frequency (Xiao *et al.* 2006). Improvements in remote sensing data gathering with increased spatial accuracy; and availability of various free satellites data provides opportunities and improve quantitative studies of activities on Earth surface for example land cover dynamics, the rate and pattern of LULC change, vegetation monitoring (Epstein *et al.*, 2002).

Many studies have been conducted on Normalized Difference Vegetation Index (NDVI) because of its usefulness in assessing vegetation, simplicity and can be easily obtained from any multispectral sensor with a visible and a near Infra-Red band, hence the reason for its general application (Huang *et al.*, 2020) for the assessment of vegetation such as land use studies, land cover changes, commercial agriculture, assessments of the climate effects on vegetation dynamics (Kalisa *et al.*, 2029); drought monitoring (Hua *et al.*, 2019, Wei *et al.*, 2021; Karnieli *et al.*, 2010; Polat *et al.*, 2024); forest health and vegetation changes (Gessner *et al.*, 2023; Kloos *et al.*, 2021; Chang *et al.*, 2022; Chrysopolitou *et al.*, 2013); monitoring land cover dynamics (Lavender, 2016); ecological environmental change (Jiang 2021); LULC changes (Hu *et al.*, 2023); systematic planning of urban environment (Guha, 2021; Guha *et al.*, 2020); and global vegetation monitoring (Roßberg & Schmitt, 2023); the study of chlorophyll concentration in leaves (Pastor-Guzman, 2015); productivity of plant (Vicente-Serrano *et al.*, 2016) and plant stress Chavez, 2016). The robustness of the NDVI-related models is directly determined by the reliability of the NDVI (Butt, 2018).

Spatial and temporal mapping of flare effects using remote sensing technology is the focus for this study. The significance of this study is to help evaluate the spatial and temporal variation of flare impact on vegetative cover detected by Landsat sensors. There are three (3) principal research questions for this study: (1). Can Landsat data be used for spatial and temporal mapping of flare effects on vegetation cover at the flare sites in the Niger Delta? (2). What is the spatial and temporal variability in the detection of flare effects on vegetation cover at each flare site? (3) How accurately can regression analysis be used for the evaluation of the flare effects on vegetation cover? Therefore, the overall aim of this study is to evaluate of the ability of Landsat 5, 7, 8 and 9 data for spatial and temporal mapping of flare effects on vegetation cover at gas flaring sites in the Niger Delta. The objectives for this study are: (1) Computation of NDVI from atmospherically corrected Landsat data for each site; (2) Regression analysis against time to produce 3 maps (Annual change in NDVI (regression slope), regression coefficient, r and p -value for the regression at each pixel for each site. (3) Computation of mean and standard deviation (SD) of NDVI for further analysis.

Materials and Methods

Study Area

Eleven (11) flaring sites including two (2) refineries (Eleme 1 and Eleme 2); seven (7) flow stations (Onne, Umurolu, Alua, Rukpokwu, Obigbo, Chokocho & Umudioga); One (1) Liquefied Natural Gas (LNG) plant (Bonny) and One (1) oil well (Sara) all from Rivers State, Niger Delta region (Figure 1) were studied for the spatial and temporal mapping of flare effects on vegetation. All sites are located within the Latitude $4^{\circ} 40' 1''$ and $5^{\circ} 01' 1''$ N and Longitude $6^{\circ} 50' 1''$ and $7^{\circ} 01' 1''$ E (Morakinyo *et al.*, 2022a; Morakinyo, 2015).

Study Data

Eleven (11) Landsat 5 TM data, forty-nine (49) Landsat 7 ETM+ data, twenty-seven (27) Landsat 8 OLI-TIRS data, and Fifteen (15) Landsat 9 OLI-TIRS data dated from 10/10/1984 to 17/12/2023 with $< 3\%$ cloud cover was used for this study. The USGS website where these data were downloaded is (<https://earthexplorer.usgs.gov/>).

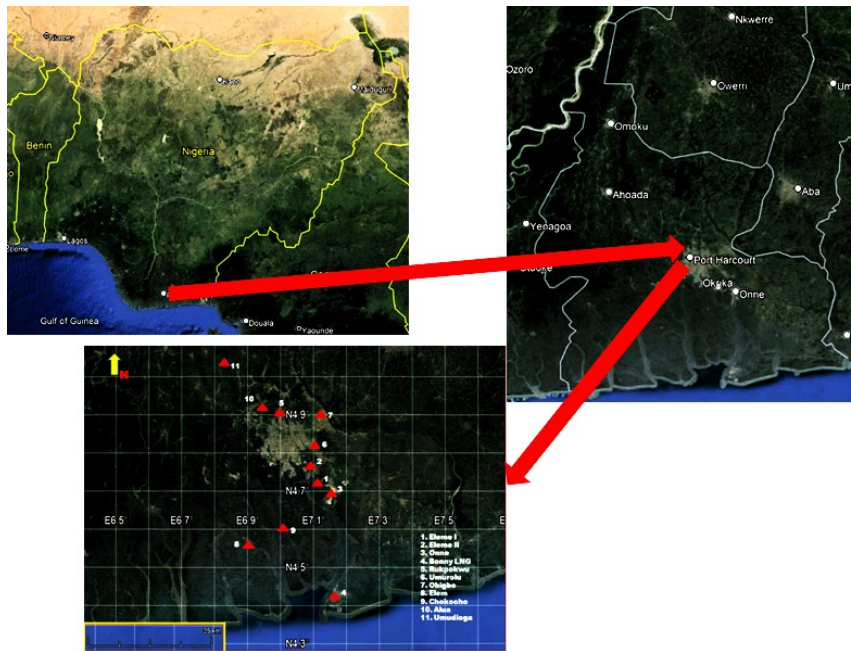


Figure 1. Above Left Map of Nigeria, (ESRI, 2024); Above Right) Map of Rivers State (ESRI, 2024); Below) 11 gas flaring studied sites (ESRI, 2024).

Methods

Processing of Landsat Data

1. Geo-location points were verified: Ten (10) ground control points (GCPs) were selected over the Niger Delta using Google Earth (Table 1). Twenty (20) images with five (5) images each from Landsat 5, Landsat 7, Landsat 8 and Landsat 9 were uploaded into the ArcGIS and the selected GCPs were identified. The comparison of the coordinates of these controls obtained from the Google Earth and ArcGIS was carried out with a negligible difference found (1.0×10^{-6} to 7.3×10^{-6} m) (Table 1). This was taken as an acceptable error range for the geo-location of the imagery.
2. Removal of zero and out of range values from the data using MATLAB code; and their replacement with not a number (nan) in order to avoid divide by zero errors in calculations. Values at the upper and lower limits of the 8-bit, 12 bit and 14 bit data range which cannot be distinguished from noise were all removed.

Table 1. Geo-location points verification for Landsat 5, 7, 8 and 9 data

S/N	Google Earth Latitude (θ)	Google Earth Longitude (λ)	Landsat 5, 7, 8 and 9 Latitude (θ)	Landsat 5, 7, 8 and 9 Longitude (λ)	Remarks
1	04 24 35.42	07 09 36.00	04 24 35.40	07 09 36.00	An edge of a two-storey building
2	04 25 48.34	07 11 15.41	04 25 48.34	07 11 15.39	A point on a tower
3	04 44 18.04	06 46 26.03	04 44 18.04	06 46 26.00	A two-point road junction
4	04 58 17.09	06 37 51.89	04 58 17.01	06 37 51.23	Edge of a fence.
5	04 52 59.09	06 52 09.95	04 52 59.09	06 52 09.00	A point on a LNG terminal
6	04 51 40.12	06 57 57.93	04 51 40.00	06 57 57.00	A three-point road junction
7	05 03 08.89	06 55 15.91	05 03 08.10	05 55 15.21	A three-point road junction
8	05 00 59.28	06 57 15.5	05 00 59.20	06 57 15.30	Edge of a building at Rivers International Airport
9	04 45 26.24	07 07 04.29	04 45 26.20	07 07 04.30	Edge of Eleme II fence
10	04 47 56.02	07 03 26.73	04 47 56.01	07 03 26.50	Edge of a building

3. The radiometric calibration of the multispectral bands of the data was done. The Digital Number (DN) values were converted to the top of atmosphere (TOA) radiance values based on the sensor calibration parameters provided within the metadata files from USGS according to the Landsat 5 (Chander & Markham, 2003), Landsat 7 (NASA, 2002), Landsat 8 and Landsat 9 Science Data Users Handbooks (Ihlen, 2019) using equations 1.

$$L_{\lambda} = ((LMAX_{\lambda} - LMIN_{\lambda}) / (QCALMAX - QCALMIN)) \times (QCAL - QCALMIN) + LMIN_{\lambda} \quad (1)$$

Where:

L_λ = Spectral radiance at the sensor's aperture ($Wm^{-2}sr^{-1}\mu m^{-1}$);
 QCAL = The quantized calibrated pixel value in DN (Digital Number);
 $LMIN_\lambda$ = Spectral radiance scaled to QCALMIN ($Wm^{-2}sr^{-1}\mu m^{-1}$);
 $LMAX_\lambda$ = Spectral radiance scaled to QCALMAX ($Wm^{-2}sr^{-1}\mu m^{-1}$);
 QCALMIN = Minimum quantized calibrated pixel value in DN = 1 for LPGS (a processing software version) products;
 QCALMAX = The maximum quantized calibrated pixel value in DN = 255.

For Landsat 8 and 9, the DN can be converted to spectral radiance using equation 2

$$L_\lambda = M_L \times Q_{cal} + A_L \quad (\text{Ihlen, 2019}) \quad (2)$$

Where:

L_λ = Spectral radiance ($Wm^{-2}sr^{-1}\mu m^{-1}$);
 M_L = Radiance multiplicative scaling factor for the band from the metadata;
 A_L = Radiance additive scaling factor for the band from the metadata;
 Q_{cal} = Level 1-pixel value in DN.

4. Computation of TOA reflectance for multispectral bands 1 to 4 for Landsat 5 and 7 including the application of simple sun angle correction is done with equation (3) which assumes Lambertian surface reflectance (NASA, 2002; Markham & Barker, 1986):

$$\rho_p = (\pi \times L_\lambda \times d^2) \div (ESUN_\lambda \times \cos \theta_s) \quad (3)$$

Where:

ρ_p = Unitless effective at-satellite planetary reflectance;
 L is measured per unit solid angle;
 πL = Upwelling radiance over a full hemisphere;
 d = Earth-Sun distance in astronomical units;
 $ESUN_\lambda$ = Mean solar exo-atmospheric irradiances;
 θ_s = Solar zenith incident angle in degrees (Chander & Markham, 2003).

For Landsat 8 and 9, Level 1 DN of multispectral bands 2-5 can be converted to TOA uncorrected reflectance for solar elevation angle using equation 4.

$$\rho_\lambda' = M_p \times Q_{cal} + A_p \quad (\text{Ihlen, 2019}) \quad (4)$$

Where:

ρ_λ' = TOA Planetary Spectral Reflectance, without correction for solar angle (Unitless);
 M_p = Reflectance multiplicative scaling factor for the band from the metadata;
 A_p = Reflectance additive scaling factor for the band from the metadata;
 Q_{cal} = Level 1-pixel value in DN.

The Landsat 8 and 9 corrected reflectance for solar elevation angle is as follows:

$$\rho_\lambda = \rho_\lambda' / \cos(\theta_{SZ}) = \rho_\lambda' / \sin(\theta_{SE}) \quad (\text{Ihlen, 2019}) \quad (5)$$

Where:

ρ_λ = TOA planetary reflectance
 θ_{SZ} = Local sun elevation angle; the scene centre sun elevation angle in degrees is provided in the metadata;
 θ_{SE} = Local solar zenith angle; $\theta_{SZ} = 90^\circ - \theta_{SE}$.

5. Atmospheric correction method: Dark object subtraction (DOS) method (Lavender, 2016, Liang et al., 2001) was adopted for this study; and it assumes within the image some pixels are in complete shadow and their radiances received at the satellite are due to the atmospheric scattering. Also, this assumption is combined with the fact that very few targets on the Earth's surface are absolute black, so an assumed 1 % minimum reflectance is better than 0 % (Chavez, 1996). Furthermore, this principle is employed for the development of algorithms for atmospheric correction for MODerate Resolution Imaging Spectroradiometer (MODIS) and Medium

Resolution Imaging Spectroradiometer (MERIS) sensors (Chavez, 1996). However, this method assumes that the error is uniform for the entire image.

With the application of DOS processes to this study, the pixels for the darkest location (Atlantic Ocean) were selected for bands 1-4 for Landsat 5 and 7, and bands 2-5 for Landsat 8 and 9 (Table 2). The computation of reflectance for these dark pixels was carried out and the lowest value recorded for each band was used as an estimate of the atmospheric reflectance for the respective band. To reduce the atmospheric effects these small errors were subtracted from the computed reflectance for each pixel of the entire image.

Table 2: Coordinates of dark pixels over Atlantic Ocean (L5, L7, L8 and L9) data

Image ID	Band 1 (Lat/Long.)	Band 2 (Lat/Long.)	Band 3 (Lat/Long.)	Band 4 (Lat/Long.)
LT51880571986017AAA04	04 20 02.07	04 20 11.21	04 21 36.79	04 21 25.05
	07 15 03.13	07 15 58.84	07 15 51.34	07 16 22.45
LT51880571987004XXX04	04 10 00.26	03 48 04.22	03 49 09.90	03 51 01.14
	07 04 43.95	07 42 00.92	07 42 01.96	07 42 23.63
LT51880571986353XXX10	04 16 48.94	04 11 40.48	04 10 16.93	04 08 08.69
	07 21 40.25	07 39 48.02	07 21 20.77	07 09 02.10
LE71880571999333AGS00	03 40 37.29	03 41 14.57	03 45 10.61	03 43 54.41
	06 35 44.23	06 35 31.92	06 34 32.91	06 32 27.08
LE71880572000352EDC00	03 57 55.38	04 17 17.76	04 18 50.68	04 19 24.42
	06 24 15.44	08 09 37.65	08 10 15.89	08 11 31.37
LE71880572003008SGS00	04 18 00.97	03 36 14.95	03 38 15.29	03 41 09.19
	07 26 14.16	07 57 22.38	07 57 45.13	07 58 49.59
		Band 2 (Lat/Long.)	Band 3 (Lat/Long.)	Band 4 (Lat/Long.)
LC81880572018361LGN00	04 22 38.41	04 22 43.01	04 22 39.58	04 22 36.42
	07 04 41.30	07 04 26.11	07 04 48.01	07 04 15.20
LC81880572019364LGN00	04 16 36.71	04 18 54.00	04 17 22.05	04 16 49.02
	08 10 10.49	08 10 32.05	08 10 47.00	08 10 19.67
LC81880572021353LGN00	03 35 25.09	03 34 22.50	03 35 44.80	03 34 19.28
	07 56 24.71	07 56 12.06	07 55 31.42	07 55 37.52
LC09L1TP18805720211211	04 22 37.00	04 23 00.05	04 22 49.61	04 22 26.08
	07 04 41.13	07 04 23.05	07 04 37.01	07 04 43.59
LC09L1T18805720220317	04 06 42.08	04 06 06.59	04 06 43.39	04 04 52.90
	06 38 18.60	06 48 45.38	06 49 22.24	06 46 54.80
LC09L1T18805720231225	03 58 05.19	03 58 42.27	03 58 57.30	03 59 11.23
	06 23 32.19	06 25 23.40	06 25 41.18	06 25 59.42

6. Atmospherically corrected reflectance: This is the result obtained after the application of DOS method in section 5 above.
7. Classification of Land Surface Cover (LSC): The atmospherically corrected reflectance bands 1-4 for Landsat 5 and 7; and bands 2-5 for Landsat 8 and 9 using the K-means function (Morakinyo et al., 2023c, Morakinyo et al., 2021, Morakinyo et al., 2020b, Şatır & Berberoğlu, 2012) of the MATLAB tool were used for the first unsupervised cluster analysis for the land cover types classification. Three (3) classes of land cover (LC) types with cloud classified as the fourth class was obtained. Any of the 3 LC (Vegetation, water, soil and built-up area) and the cloud as the fourth class were identified. Also, MATLAB codes were used for the elimination of the cloud class by masking. The cloud-masked reflectance was used for the second cluster analysis and 4 LC retrieved are vegetation, soil, built up area and water (Morakinyo et al., 2021, Maaharjan, 2018, Morakinyo, 2015). However, Landsat SWIR bands 5 and 7 (Landsat 5 and 7), and bands 6 and 7 (Landsat 8 and 9) were also employed for the classification of land cover types but they could not give useful results as the bands used, therefore, they were dropped for further analysis. Furthermore, Visual examination of Worldview-1 and 2, and IKONOS pseudo-true colour images (RGB) from Google Earth and Digital Global (<http://browse.digitalglobe.com/imagefinder/public.do>) were also used to study and clarified the LC obtained. Results obtained from LC classification were used to summarize the LC types around each site.

8. Retrieval of Normalized Differential Vegetation Index (NDVI) in the N, E, S and W directions: The cloud-masked reflectance bands 3 and 4 for Landsat 5 and 7, and bands 4 and 5 for Landsat 8 and 9 were used for the retrieval of NDVI (Morakinyo *et al.*, 2023a). For Landsat 5 and 7, band 3 is Red (R) and band 4 is Near Infra-Red (NIR) while for Landsat 8 and 9, band 4 is R and band 5 is NIR. Mathematical formula for NDVI is as stated in equation (6) (Huete *et al.*, 2002).

$$\text{NDVI} = (\text{NIR} - \text{R}) / (\text{NIR} + \text{R}) \quad (6)$$

Where,

NIR = Near Infra-Red reflectance;

R = Red reflectance.

The MATLAB codes used for data processing and analyses in this study are implemented as follow:

Retrieval of reflectance

- Each imagery was read from the folder i.e. a folder was created for Landsat 5, Landsat 7, Landsat 8, and Landsat 9 respectively. 1 = L5_folder310513; 2 = L7_folder010613; 3 = L8_folder020613; and 4 = L9_folder030613;
- Read in XL radiometric calibration file; fill in all gaps in XL file with Nan (i.e. Not a number).
- For each Scene Name, convert the specific characters into numerical path, row, year, day.
- Plot (scene Path, 'x'); plot (scene Year, 'X'); plot (scene Day, 'X')
- Read Landsat data files;
- Read .mtl files;
- Write a loop to automatically go through each line of the file. Instead of printing out;
- This process is repeated from while to the line counter to process for each X & Y;
- Choice of dimension of area around the flare station for investigation; i.e. the 12 × 12 km;
- Removal of zero values or bad values;
- Dark pixel method of Atmospheric Correction for the Landsat reflective bands;
- Channel the reading of both scene and radiometric calibration files;
- Radiometric calibrations for multispectral bands 1, 2, 3 and 4 for Landsat 5, and Landsat 7; and bands 2, 3, 4, and 5 for Landsat 8, and Landsat 9.
- Convert digital numbers (DN) back to the top-of-atmosphere radiances (Lt) for all Landsat bands.
- Computation of at sensor radiance for dark pixels
- Apply a simple sun angle correction to calculate reflectance Rt at the flaring sites from the top-of-atmosphere radiance
- Application of atmospheric correction to reflective bands 1-4
- Computation of dark pixel reflectance for bands 1-4 for Landsat 5 and Landsat 7; and bands 2-5 for Landsat 8 and 9;
- True reflectance for bands 1 to 4 1-4 for Landsat 5 and Landsat 7; and bands 2-5 for Landsat 8 and 9 i.e. application of atmospheric correction;

Cluster processing (I)

- k-means for unsupervised and supervised land cover classifications;
- Application of MATLAB 'Statistics Toolbox' for k-means clustering;

Masking of cloud

- To identify cloud and mask it from the data;

Cluster processing (II) & Land cover classifications

- To look at the four (4) classes as a map;
- To look at the centroid and range of each band and each cluster;
- And compare the 'spectra' for the 4 classes:
- To give each land cover classification as vegetation; water; soil; built up

Retrieval of Normalized Differential Vegetation Index (NDVI)

- Computation of the NDVI;
- NDVI for vegetation i.e. Masking of water, soil and built up classes to remain only vegetation;
- Computation of mean NDVI for vegetation;

Conversion from Julian day to month and day

- Formal function for converting julian day into month + day;

- Month for a given year (leap / not leap year);
- Years divisible by 4 are leap years;
- Catch days in January;

Spatio-temporal regression analysis

- Create a directory for the results files;
- Stop at 307 for the processing of NDVI;
- Load(d1(ifile).name, 'ndvi_mask', 'IDX3','water', 'vegetation', 'builtup', 'soil') ;
- Conversion to julian days
- Initialize output variables: slopes(ibad) = nan; rvalues(ibad) = nan; pvalues(ibad) = nan; n(ibad) = nan;
- Plot the maps: Slope, r-values and p-values maps respectively;
- print('-f150','-r600','-dpng', 'spatial_regression_Stn_1.png').

A summary of stages for the processing of Landsat 5, 7, 8 and 9 is shown in Figure 2.

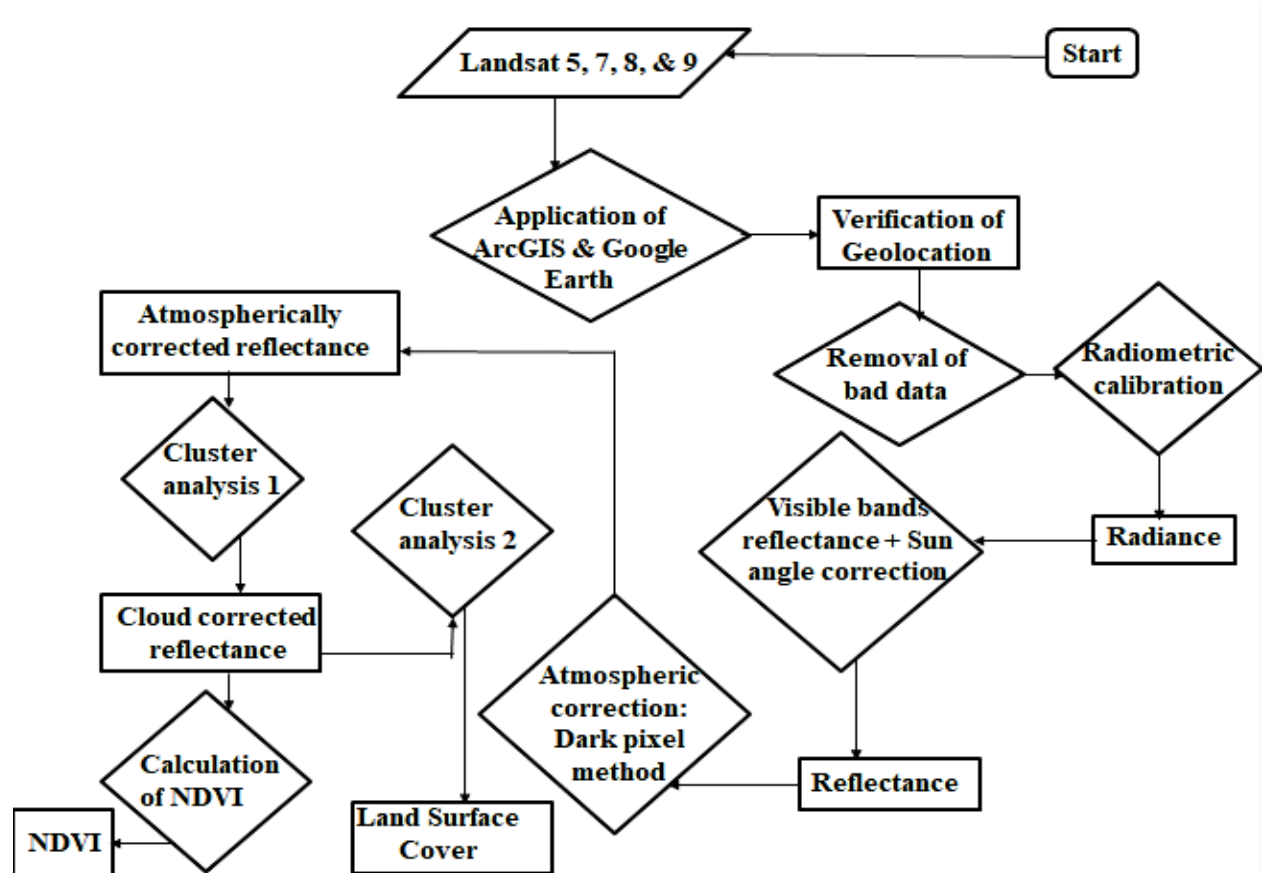


Figure 2. Methodology for processing of Landsat 5, 7, 8 and 9 data.

In situ measurement for validation of Landsat data

Methods and processes for the evaluation of satellite data to check if such data meet their stated accuracy requirements and objectives is referred to as the validation of satellite products. For this study, the validation measurements were carried out at Eleme Refineries I and II, and Onne, Alua, Chokocho & Obigbo Flow Stations on 27/07/2012 for reconnaissance activities. On 04/08/2012 to 21/09/2012 (Morakinyo, 2015), the first ground measurements and observations took place; and were also repeated from 05/08/2019 to 22/09/2019 (Morakinyo, 2025b; Morakinyo, 2024a, b, c; Morakinyo *et al.*, 2021). The third field measurement occurred from 05/08/2023 to 22/09/2023. The insitu data acquired are coordinates of features and points, relative humidity, air temperature, and photographs of features and locations. In addition, fieldwork activities at these 6 flaring sites confirmed that their LC (vegetation, some buildings, open land and water bodies) types are similar; and that they are the same

with all other remaining flaring sites examined due to the similarity in the topography of the Niger Delta.

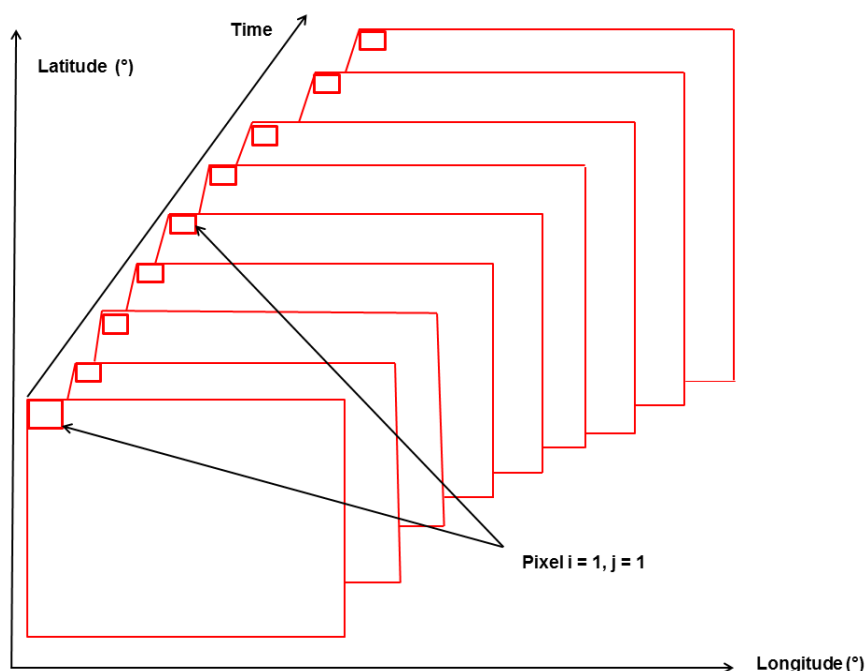


Figure 3. Schematic diagram for spatio-temporal analysis

Results and Discussion

Retrieval of NDVI

NDVI values were obtained for each pixel covering each site of 12 by 12 km i.e. 400 × 400 pixel.

Regression Analysis

This analysis is necessary in order to evaluate the spatial and temporal variation in detection of flare effects on the vegetation cover by Landsat data (Figure 3). The spatially-resolved linear regression of NDVI against time from 1984 to 2023 for each site was carried out for the purpose of generating three maps for each site (Annual change in NDVI (regression slope), regression coefficient, *r* and *p*-value for the regression at each pixel). Data calculated are mean (positive (+), negative (–) and all) and standard deviation (SD) (positive (+), negative (–) and all) of NDVI trend values. Tables 3-13 presents the mean and SD for (+), (–) and net slopes of NDVI at each site.

Table 3. Eleme 3: Mean and SD for (+), (–) and net slopes of NDVI (Change in NDVI/ year).

S/N	Parameters	Value obtained
1.	Mean (pixels with + slope)	2.3164×10^{-5}
2.	Mean (pixels with – slope)	-2.7076×10^{-5}
3.	SD (pixels with + slope)	3.3855×10^{-5}
4.	SD (pixels with – slope)	3.8550×10^{-4}
5.	Mean (all)	1.9166×10^{-5}
6.	SD (all)	2.0689×10^{-4}

Table 4. Eleme 2: Mean and SD for (+), (–) and net slopes of NDVI (Change in NDVI/ year).

S/N	Parameters	Value obtained
1.	Mean (pixels with + slope)	2.0741×10^{-5}
2.	Mean (pixels with – slope)	-1.7400×10^{-4}
3.	SD (pixels with + slope)	3.0926×10^{-5}
4.	SD (pixels with – slope)	2.5439×10^{-4}
5.	Mean (all)	1.5010×10^{-5}
6.	SD (all)	1.3596×10^{-4}

Table 5. Onne: Mean and SD for (+), (–) and net slopes of NDVI (Change in NDVI/ year).

S/N	Parameters	Value obtained
1.	Mean (pixels with + slope)	1.0817×10^{-5}
2.	Mean (pixels with – slope)	-2.4278×10^{-5}
3.	SD (pixels with + slope)	2.9639×10^{-5}
4.	SD (pixels with – slope)	1.0757×10^{-4}
5.	Mean (all)	2.2849×10^{-6}
6.	SD (all)	7.9515×10^{-5}

Table 6. Umurolu: Mean and SD for (+), (–) and net slopes of NDVI (Change in NDVI/ year).

S/N	Parameters	Value obtained
1.	Mean (pixels with + slope)	5.8684×10^{-5}
2.	Mean (pixels with – slope)	-1.6787×10^{-5}
3.	SD (pixels with + slope)	3.7938×10^{-5}
4.	SD (pixels with – slope)	4.2276×10^{-4}
5.	Mean (all)	5.8057×10^{-5}
6.	SD (all)	7.4988×10^{-5}

Table 7. Bonny: Mean and SD for (+), (–) and net slopes of NDVI (Change in NDVI/ year).

S/N	Parameters	Value obtained
1.	Mean (pixels with + slope)	2.4228×10^{-5}
2.	Mean (pixels with – slope)	-3.0889×10^{-5}
3.	SD (pixels with + slope)	3.3757×10^{-5}
4.	SD (pixels with – slope)	1.8121×10^{-4}
5.	Mean (all)	2.1294×10^{-5}
6.	SD (all)	8.2903×10^{-5}

Table 8. Alua: Mean and SD for (+), (–) and net slopes of NDVI (Change in NDVI/ year).

S/N	Parameters	Value obtained
1.	Mean (pixels with + slope)	8.8056×10^{-5}
2.	Mean (pixels with – slope)	-2.4815×10^{-4}
3.	SD (pixels with + slope)	5.2640×10^{-5}
4.	SD (pixels with – slope)	0.0011
5.	Mean (all)	8.7469×10^{-5}
6.	SD (all)	1.4516×10^{-4}

Table 9. Rukpokwu: Mean and SD for (+), (–) and net slopes of NDVI (Change in NDVI/ year).

S/N	Parameters	Value obtained
1.	Mean (pixels with + slope)	7.6961×10^{-5}
2.	Mean (pixels with – slope)	-4.3011×10^{-5}
3.	SD (pixels with + slope)	4.1556×10^{-5}
4.	SD (pixels with – slope)	1.7924×10^{-4}
5.	Mean (all)	7.3986×10^{-5}
6.	SD (all)	6.2093×10^{-5}

Table 10. Obigbo: Mean and SD for (+), (–) and net slopes of NDVI (Change in NDVI/ year).

S/N	Parameters	Value obtained
1.	Mean (pixels with + slope)	7.9023×10^{-5}
2.	Mean (pixels with – slope)	-3.5435×10^{-4}
3.	SD (pixels with + slope)	4.5078×10^{-5}
4.	SD (pixels with – slope)	7.1281×10^{-4}
5.	Mean (all)	7.8273×10^{-5}
6.	SD (all)	1.1192×10^{-4}

Figures 4-14 show Maps of annual change in NDVI (regression slopes), regression coefficient, *R*-values and *p*-values for each of the flaring site are presented in Figs 4-14. $\alpha > 0.05$ is the significant level adopted for the analysis. The *p*-value maps are *P*s which shows where the relationship is

statistically significant. The yellow colour area in the map slope shows portions within the site where the temporal trend in NDVI is statistically significant. Also, portions that are always cloudy or that are not vegetation are white in the map P.

Table 11. Chokocho: Mean and SD for (+), (–) and net slopes of NDVI (Change in NDVI/ year).

S/N	Parameters	Value obtained
1.	Mean (pixels with + slope)	1.0546×10^{-4}
2.	Mean (pixels with – slope)	-2.1310×10^{-4}
3.	SD (pixels with + slope)	3.9183×10^{-5}
4.	SD (pixels with – slope)	4.3901×10^{-5}
5.	Mean (all)	1.0520×10^{-4}
6.	SD (all)	5.0786×10^{-5}

Table 12. Umudioga: Mean and SD for (+), (–) and net slopes of NDVI (Change in NDVI/ year).

S/N	Parameters	Value obtained
1.	Mean (pixels with + slope)	4.8557×10^{-5}
2.	Mean (pixels with – slope)	-4.0582×10^{-5}
3.	SD (pixels with + slope)	5.8950×10^{-5}
4.	SD (pixels with – slope)	8.9129×10^{-5}
5.	Mean (all)	-3.0408×10^{-5}
6.	SD (all)	1.0120×10^{-4}

Table 13. Sara: Mean and SD for (+), (–) and net slopes of NDVI (Change in NDVI/ year).

S/N	Parameters	Value obtained
1.	Mean (pixels with + slope)	3.3600×10^{-5}
2.	Mean (pixels with – slope)	-2.9388×10^{-5}
3.	SD (pixels with + slope)	2.4634×10^{-5}
4.	SD (pixels with – slope)	9.2132×10^{-5}
5.	Mean (all)	1.4015×10^{-5}
6.	SD (all)	7.6382×10^{-5}

For Figure 4 (Eleme Refinery I) there is a little portion with yellow colour in the slope map which spread in the N, E, S and NW directions within the site that presented significant temporal trend in the NDVI. -2.71×10^{-5} - 2.32×10^{-5} is the range of value with a mean of $\pm 3.38 \times 10^{-5}$ and the p-value is from 0.05 and above. However, the significant trend for a small portion occurred (slope map) in the NW, S and SW directions within the site Eleme Refinery II Figure 5); and the value obtained ranges from $(-1.740 \times 10^{-4}$ - $2.074 \times 10^{-5})$ with a mean of $(\pm 3.093 \times 10^{-5})$ and p-value from 0.05 and above. For Onne station (Figure 6), little portions in the E, SE, S and W directions presented a significant result. The range of the trend in NDVI is $(-2.428 \times 10^{-5}$ - $2.9639 \times 10^{-5})$ with SD of $(\pm 7.952 \times 10^{-5})$ and p-value from 0.05 and above.

Figure 7 (Umurolu) slope shows that there is a significant positive temporal trend in NDVI within Umurolu site (portion with yellow colour). The spatially coherent portion in NDVI within the Umurolu site which include boundary of the flow station and an area within the site up to a distance of 90 m from the flare (mostly E direction) is between $(-1.679 \times 10^{-5}$ and $5.868 \times 10^{-5})$ with SD of $(\pm 7.499 \times 10^{-5})$; and with the p-value from 0.05 and above. For Figure 8 (Bonny LNG) some portions within the site in the N, NE, E, S and SE directions (area with yellow colour) gives significant results with -3.089×10^{-5} - 2.423×10^{-5} as the range of NDVI and the same p-value as for Umurolu. Also, Alua site (Figure 9) presented a significant result around the flow station and at a distance towards E, NE, W and NW directions (sections with yellow colour) where the slope $\neq 0$ (between -2.482×10^{-4} - 8.806×10^{-5} , with a SD $\pm 1.452 \times 10^{-4}$); and p-value from 0.05 and above.

Rukpokwu (Fig. 10) has significant trend in NDVI with the locations that are spatially coherent (portions with yellow colour). Such portions are around the facility, towards N, NW and SW where the changes in NDVI are more pronounced. NDVI range for Rukpokwu is $(-4.301 \times 10^{-5}$ - $7.696 \times 10^{-5})$, SD of $(\pm 6.209 \times 10^{-5})$ and value of p is 0.05 and above. In addition, Obigbo (Figure 11) also show statistically significant results (yellow colour portions) with much effect in the N, NE, E and S. NDVI is $(-3.544 \times 10^{-4}$ - $7.902 \times 10^{-5})$, SD $(\pm 1.119 \times 10^{-4})$ and p-value is 0.05 and above. For Chokocho (Figures 12) most portions such as flow station surroundings within the site presented significant results Chokocho's NDVI range in the trend is $(-2.131 \times 10^{-4}$ - $1.055 \times 10^{-5})$, SD $(\pm 5.079 \times 10^{-5})$, and p-value is 0.05 and above.

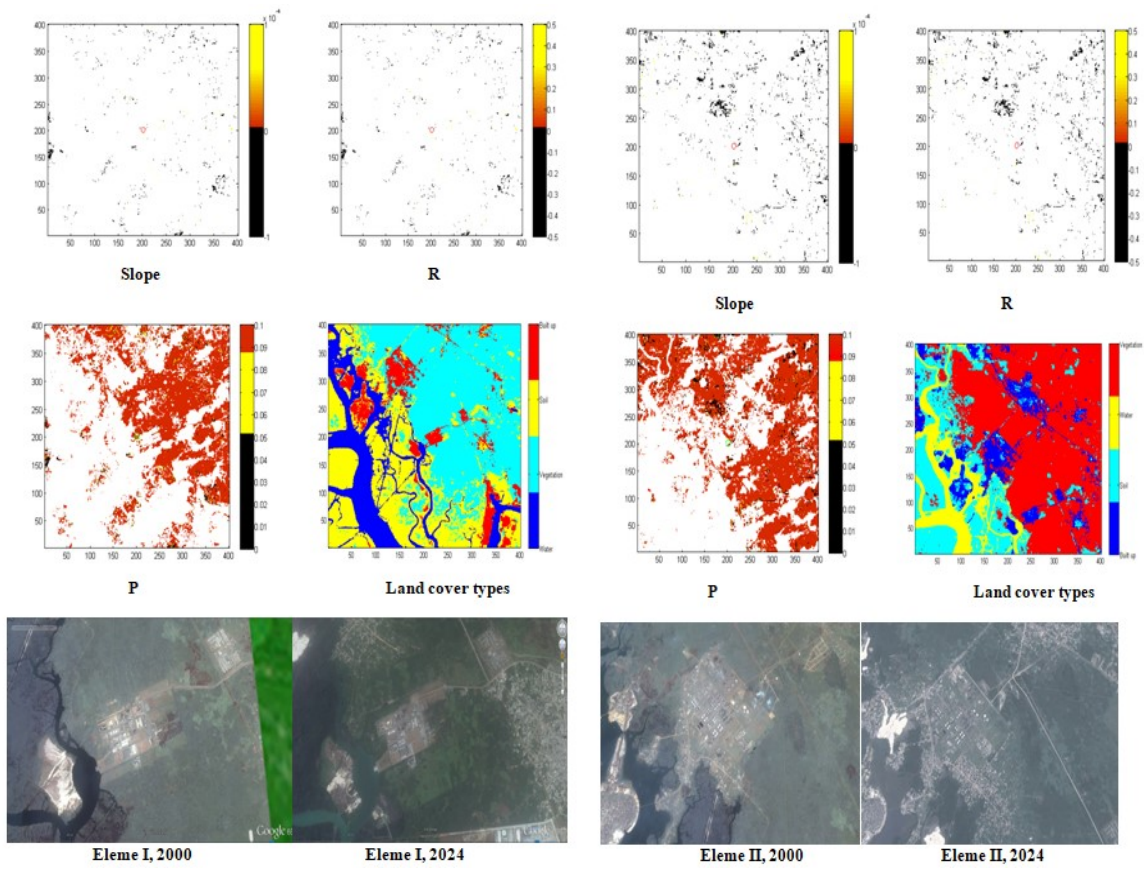


Figure 4. Maps of slope, r & p values; & land cover types for Eleme I

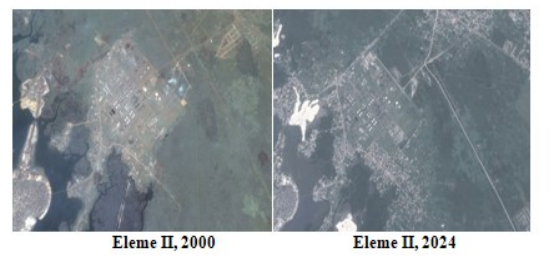


Figure 5. Maps of slope, r & p values; & land cover types for Eleme II

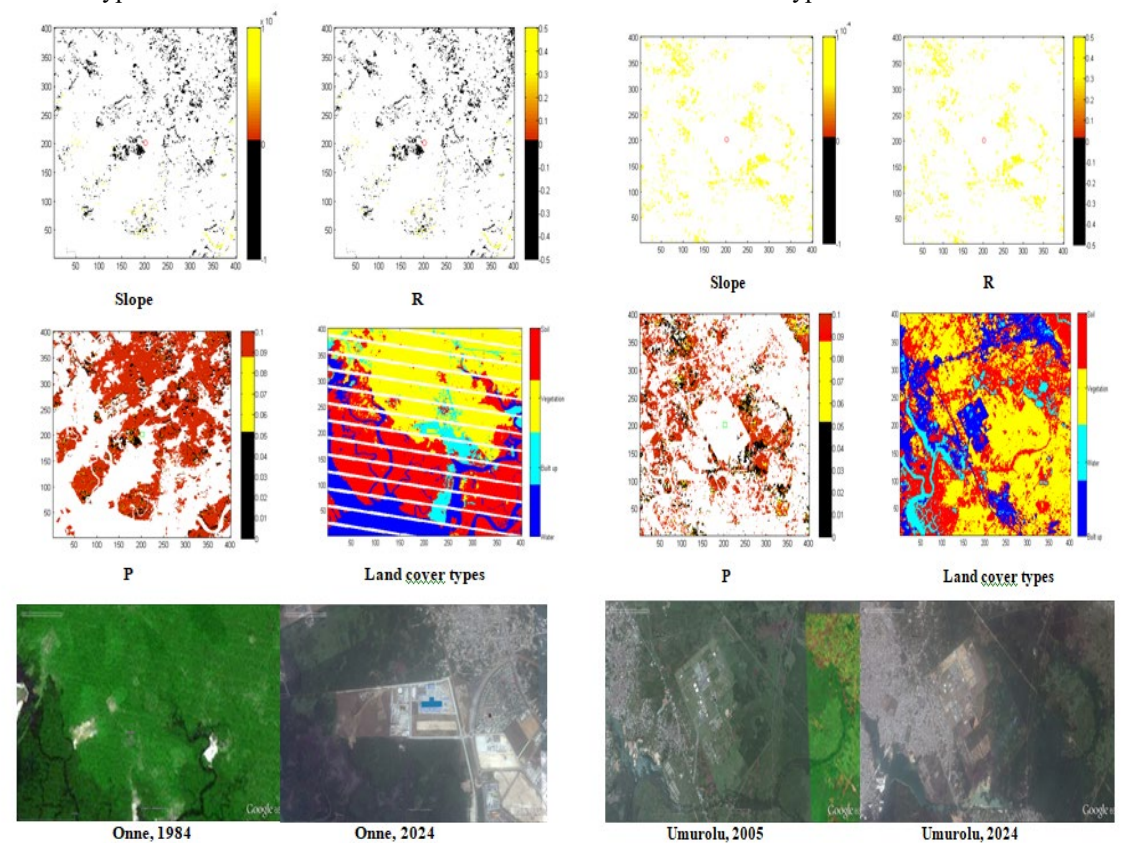


Figure 6. Maps of slope, r & p values; & land cover types for Onne

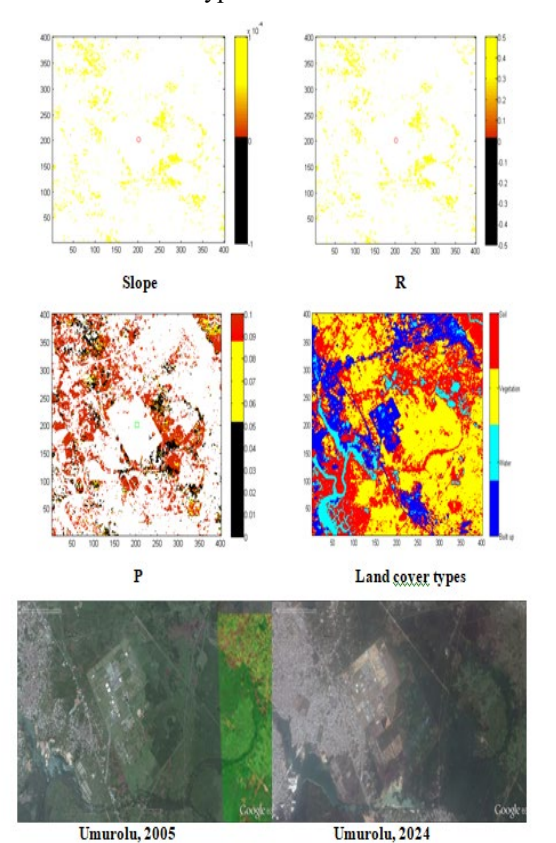


Figure 7. Maps of slope, r & p values; & land cover types for Umurolu

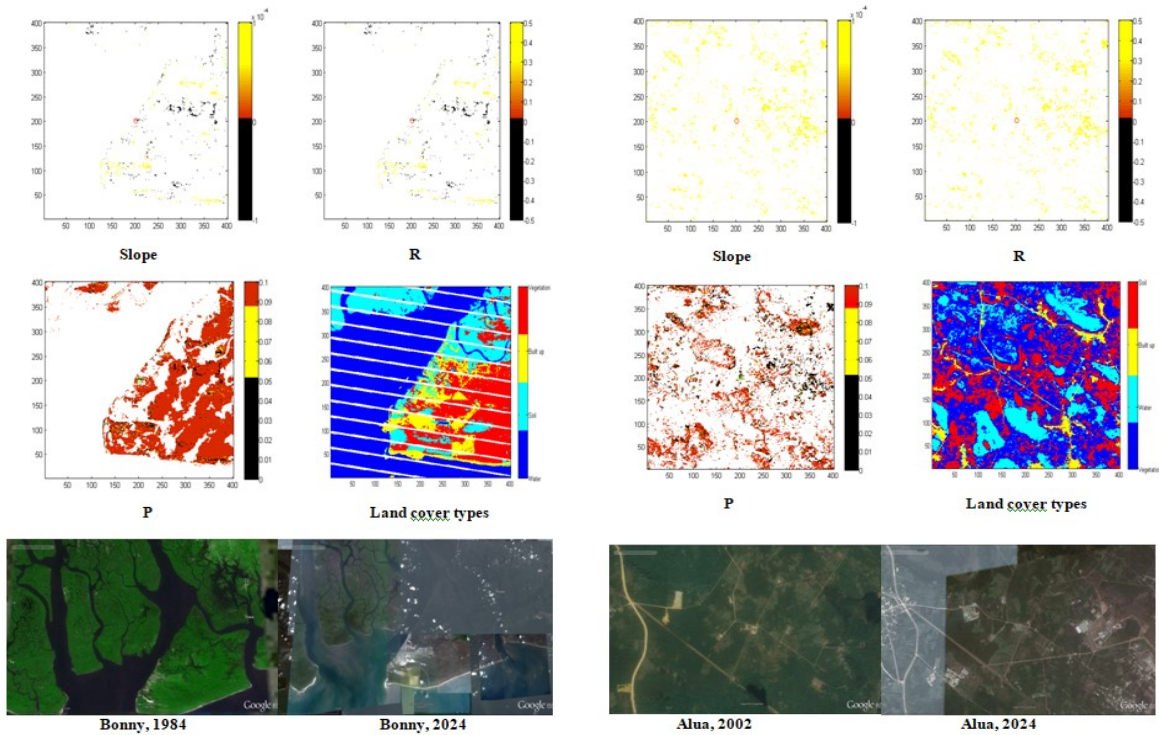


Figure 8. Maps of slope, r & p values; & land cover types for Bonny

Figure 9. Maps of slope, r & p values; & land cover types for Alua

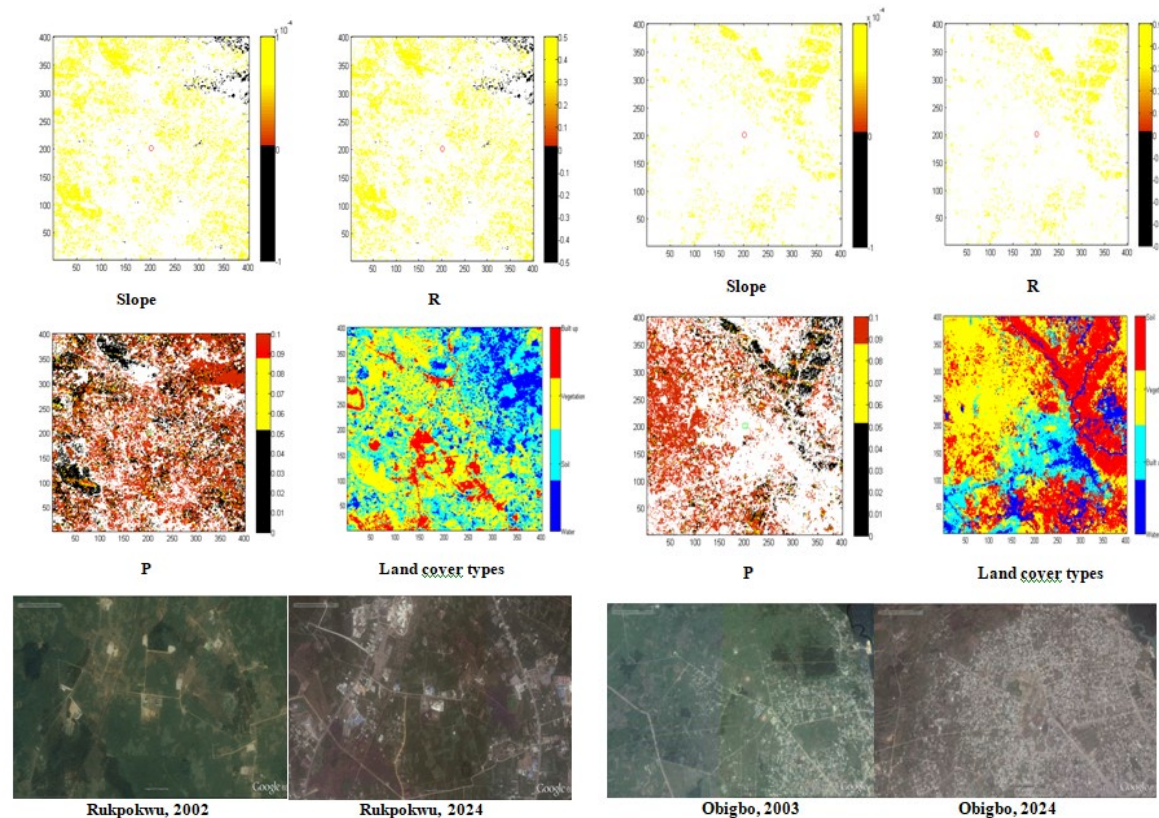


Figure 10. Maps of slope, r & p values; & land cover types for Rukpokwu

Figure 11. Maps of slope, r & p values; & land cover types for Obigbo

For Figure 12 slope, sufficient data to proof that the gas flaring effects only is the factor for the trend in NDVI throughout the site. Factors such as burning of refuse, clearing of bush for farming, burning of bush for killing of animals etc could be contributing to the result.

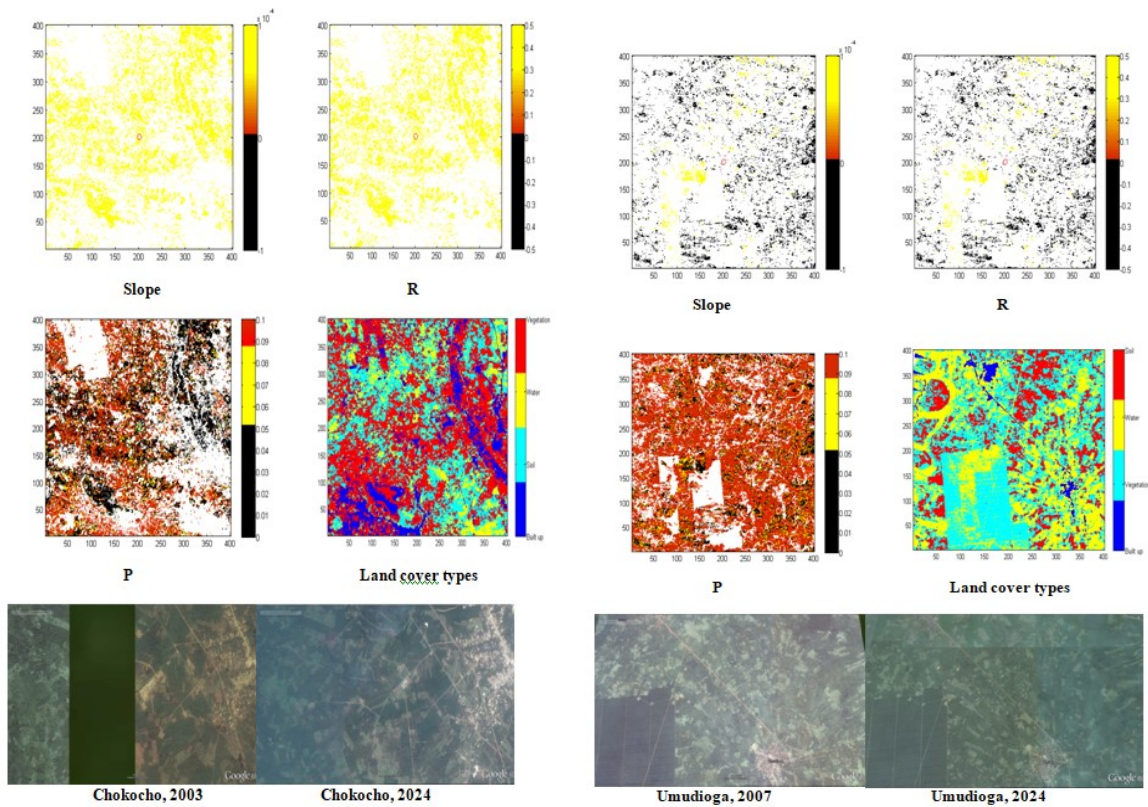


Figure 12. Maps of slope, r & p values; & land cover types for Chokocho

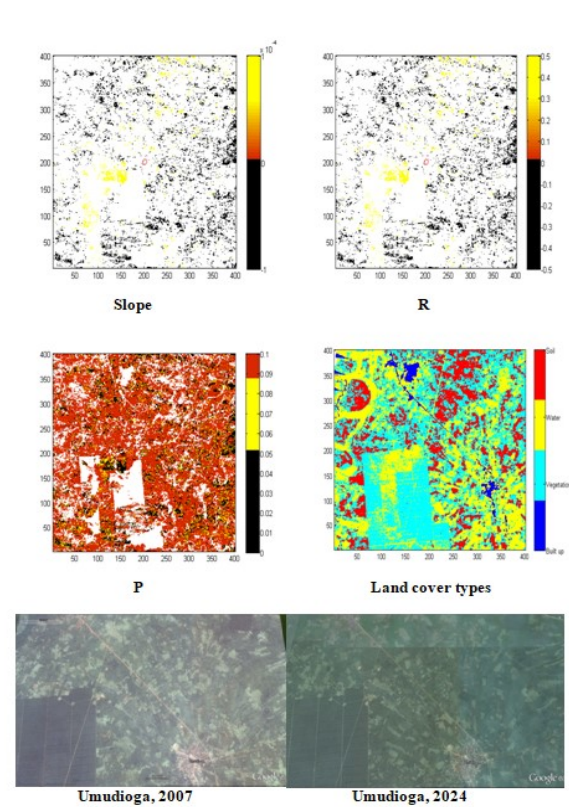


Figure 13. Maps of slope, r & p values; & land cover types for Umudioga

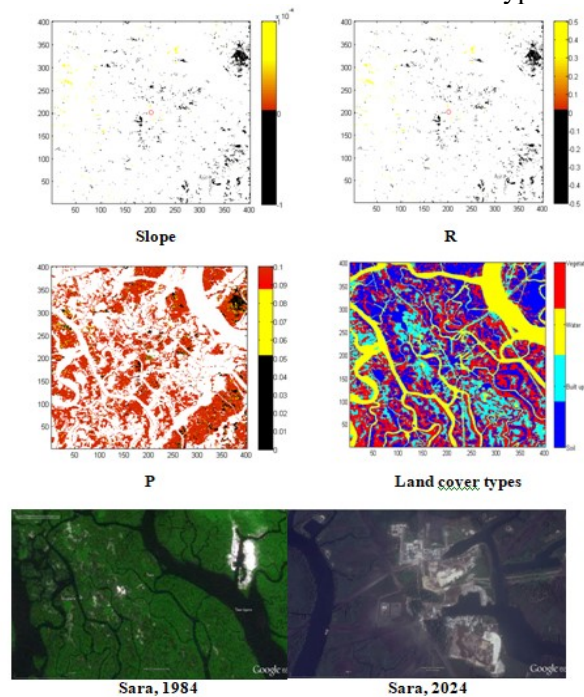


Figure 14. Maps of slope, r & p values; & land cover types for Sara

Umudioga (Figure 13) presented statistically significant results within the site which is more pronounced around the facility towards W except in the NW direction. The N of the site shows a partially significant trend. The NDVI trend range for the site is $(-4.058 \times 10^{-5} - 4.856 \times 10^{-5})$, SD $(\pm 1.012 \times 10^{-4})$ and p-value is 0.05 and above. Furthermore, Sara site (Figures 14), located at the coastal boundary of River Bonny presented that a little portion within the site has a statistically significant result with not much in the S and SW directions. The result obtained could be as a result of

its coastal location. NDVI trend range (-2.939×10^{-5} - 3.360×10^{-5}), SD (7.638×10^{-5}), and p-value of 0.05 and above are recorded.

The significant (+) trends results in the NDVI for a larger area within each site were presented by the inland facilities (Umurolu, Alua, Rukpokwu, Obigbo, Chokocho and Umudioga). Coastal facilities (Bonny, Eleme I and II, Onne, and Sara) show the significant (+) trends in the NDVI over a small area. However, Bonny facility show wider (+) significant trend than all other coastal facilities because it has 5 flare stacks within the facility. Also, for Bonny site the + significant trend in the E direction of the site could be as a result of the impact of human activities e.g. urban growth.

The results show that the temporal in NDVI is specific to each site, and that the effect of the flares on the vegetation cover does not majorly depend on the size of facility. Both Eleme I (-2.71×10^{-5} - 2.32×10^{-5}) and II (-1.740×10^{-4} - 2.074×10^{-5}) presented significant results for a small portion of the area. Umurolu (-1.679×10^{-5} - 5.868×10^{-5}) and Bonny (-3.089×10^{-5} - 2.423×10^{-5}) show significant results which could be as a result of the number of flare stacks within them 4 and 5 respectively. Furthermore, all small and medium facilities show statistically significant results which could be attributed to the rate and volume of gas burning from them. Sara site with statistically significant results (-2.939×10^{-5} to 3.360×10^{-5}) over a narrow area is a result of its swampy location with many tributaries.

The results of previous studies similar to this research are in support of the results obtained for this research. From Figures 4-14, the marked yellow colour portions in the slope maps shows the area within the site where the NDVI temporal trend is statistically significant. This means that as a result of nearly zero or lowest value of NDVI, the vegetation is sparse, nearly dead or dead due to the effect of gas flaring in the area. This is supported by several researchers including Nwaogu & Onyeze (2020); they stated that destruction of vegetation and agricultural produce are some of impacts of flaring in the environment. Musa et al. (2024) also concluded that stunted growth, death of vegetation and farm produce are part of results of flaring gas effects in the environment. Furthermore, Lu et al. (2020); Umbugala & Morakinyo (2023); Morakinyo (2024a); Morakinyo (2025b) concluded that environmental pollution occurs at flaring sites. In addition, many researchers have concluded that NDVI is the most useful vegetation index for vegetation assessment. Other previous results that are in supports of this study includes (Kalisa et al., 2019); Huang et al., 2020; Hua et al., 2019, Wei et al., 2021; Karnieli et al., 2010; Polat et al., 2024; Gessner et al., 2023; Kloos et al., 2021; Chang et al., 2022; Chrysopolitou *et al.*, 2013); Lavender, 2016); Jiang, 2021); Hu et al., 2023; Guha, 2021; Guha et al., 2020; Roßberg & Schmitt, 2023; Pastor-Guzman, 2015; Vicente-Serrano et al., 2016; Chavez, 2016).

The limitation of this study is that Landsat data used cover only dry season in Nigeria. Hence, the results obtained cannot determine the effects of the flare on the vegetation in all seasons. How each vegetation type responds to the flare could not be assessed due to lack of data on the vegetation types and their photosynthetic rate. The rate and volume of the gas burning at each site does could not be applied to this study due to their unavailability and so this study could not give the exact total influence of flare on the vegetation.

Conclusions

Generally, the results show a fall from healthy vegetation as the flare stacks are being spatially approached in the all sites and so the vegetation closer to the flare is dead. The impact of gas flare is felt up to 120 m from the stack with an annual reduction in NDVI values over the timescale analyzed. Onne site show an unstable trend from 1984 to 2007 (years before it was built) which could be as a result of vegetation density, vegetation types and their photosynthetic rate as there was no flaring activities during this period.

The results obtained show that each site is specific with its own temporal trend in NDVI from 1984 to 2024. Hence, it can be concluded that Landsat data can be used to map the spatial and temporal impacts of flare on vegetation cover in the Niger Delta. However, the spatial and temporal variability in Landsat data linked to the detectable flare impact on vegetation cover is specific to each site and its activities, and dependent on the landscape of the site, e.g. Sara facility is built in the swampy terrain. Flaring is still ongoing in Nigeria and its associated challenges evident with Nigerian Government yet to determine to have zero flare in Nigeria. Therefore, I wish to make the following recommendations:

- Nigerian Government should carry out the stringent enforcement of the Nigerian Petroleum Industry Act of 2021.
- Nigerian Environmental protection laws should have adequate provisions for combating oil and gas pollution, degradation, and gas flaring. The National Environmental Standard Regulation Enforcement Agency (Establishment) Act (NESREA), 2007, should be amended to widen its scope to oil and gas sector activities.
- The Nigerian Constitution should be amended to make environmental infringements justiciable in order to guarantee a healthy and sustainable environment.
- Enactment of the comprehensive regulatory framework governing gas utilization and development of gas pipeline networks to all the six (6) geo-political zones in Nigeria for proper gas distribution.
- The Nigerian Government should increase generation of electricity in Nigeria using gas.
- Oil companies should update their equipment to modern technologies and methods to be in accordance with the international standards.
- Nigerian Government should encourage investors in the energy sector by providing the enabling environment.
- A gas flaring price targeting natural gas companies should be more effective in mitigating gas flaring than the wider 'carbon price' or pollution price/tax policy.
- The Federal Government should provide alternative energy sources to mitigate the effect of gas flaring on the people and salvage the environment.

Acknowledgement: The Author is grateful to the USGS for the provision of Landsat data. Many thanks to Jill Schwarz for MATLAB coding and guidance.

Conflict of Interest: The Author declares no conflict of interest.

References

- Berlanga-Robles CA, Ruiz-Luna A, (2002). Land use mapping and change detection in the coastal zone of northwest Mexico using remote sensing techniques. *J. Coastal Resour.* **18**(3):514-522. <https://www.jstor.org/stable/4299098>
- Butt B, (2018) Environmental indicators and governance. *Current Opinion on Environ. Sus.* **32**: 84-89. <https://doi.org/10.1016/j.cosust.2018.05.006>
- Campbell JB, (2007) Introduction to remote sensing, 4thEdn. The Guilford Press, New York. <https://istnrcg.wordpress.com/wp-content/uploads/2019/09/introduction-to-remote-sensing-www.gisman.ir.pdf>
- Chander G, Markham K, (2003). Revised Landsat 5 TM Radiometric Calibration Procedures and Post Calibration Ranges. *IEEE Trans. of Geosci. & Remote Sens.* **41**(11): 2674-2677. <https://doi.org/10.1109/TGRS.2003.818464>
- Chang J, Liu Q, Wang S, Huang C, (2022) Vegetation Dynamics and Their Influencing Factors in China from 1998 to 2019. *Remote Sensing* **14**, 3390. <https://doi.org/10.3390/rs14143390>
- Chavez PS, (1996) Image-based Atmospheric Corrections-Revisited and Improved. *Photogrammetry Engineering & Remote Sensing* **62**(9): 1025-1036. https://www.researchgate.net/publication/236769129_Image-Based_Atmospheric_Corrections_-_Revisited_and_Improved
- ChrysopolitouV, ApostolakisA, AvtzisD, AvtzisN, DiamandisS, KemitzoglouD, PapadimosD, PerlerouC, TsiaoussiV, DafisS, (2013) Studies on forest health and vegetation changes in Greece under the effects of climate changes. *Biodiv. Conser.*, **22**:1133-1150, <https://link.springer.com/article/10.1007/s10531-013-0451-2>.
- Epstein J, Payne K Kramer E, (2002) Techniques for mapping suburban sprawl. *Photogrammetry Engineering Remote Sensing* **68**(9):913-918 EROS (2021) Earth Resources Observation and Science (EROS)
- ESRI. (2024) Map of Nigeria, map of Rivers State and map of 11 gas flaring studied sites. <https://www.esri.com/en-us/arcgis/products/arcgis-storymaps/contest/overview>
- Gessner U, Reinermann S, Asam S, Kuenzer C, (2023) Vegetation Stress Monitor-Assessment of Drought and Temperature-Related Effects on Vegetation in Germany Analyzing MODIS Time Series over 23 Years. *Remote Sensing* **15**, 5428. <https://doi.org/10.3390/rs15225428>
- Guha S, (2021) A long-term monthly assessment of land surface temperature and normalized difference vegetation index using Landsat data. *urbe. Revista Brasileira de Gestão Urbana*, v.13, e20200345. <https://doi.org/10.1590/2175-3369.013.e20200345>

- Guha S, GovilH, DiwanP, (2020) Monitoring LST-NDVI Relationship Using Premonsoon Landsat Datasets. *Advan. in Meteo.*2020, Article ID 4539684, 15 <https://doi.org/10.1155/2020/4539684>
- Hu Y, Raza A, Syed, NR, AcharkiS, Ray RL, Hussain S, Dehghanisanij H, Zubair M, Elbeltagi A, (2023) Land Use/Land Cover Change Detection and NDVI Estimation in Pakistan's Southern Punjab Province. *Sustain.*, 15, 3572,<https://doi.org/10.3390/su15043572>
- HuaX, RenaH, TanseyK, ZhengaY, GhentD, LiuX, YanL, (2019) Agricultural drought monitoring using European Space Agency Sentinel 3A land surface temperature and normalized difference vegetation index imageries. *Agri.& Forest Meteor.*279, 107707. <https://www.scilit.com/publications/ab36ace649bb150860f2a1b0058149ec>
- HuangS, TangL, HupyP, WangY, ShaoG, (2020) A commentary review on the use of normalized difference vegetation index (NDVI) in the era of popular remote sensing. *J. Forestry Res.* 32(1): 1-6,<https://doi.org/10.1007/s11676-020-01155-1>
- HueteA, DidanK, MiuraT, RodriguezEP, X Gao, FerreiraLG, (2002) Overview of the radiometric and biophysical performance of the MODIS vegetation indices. *Remote Sens. Environ.* 83 (1-2): 195-213. [https://doi.org/10.1016/S0034-4257\(02\)00096-2](https://doi.org/10.1016/S0034-4257(02)00096-2)
- IhlenV, (2019) Landsat 8 (L8) Data Users Handbook, Version 5.0. Department of the Interior, U.S. Geological Survey. <https://www.usgs.gov/landsat-missions/landsat-8-data-users-handbook>
- Jensen JR, (2005) Introductory digital image processing: a remote sensing perspective, 3rd edn. Prentice Hall, Upper Saddle River Campbell JB (2007) Introduction to remote sensing, 4thedn. The Guilford Press, New York. <https://www.scribd.com/document/667034923/JENSEN-J-R-Introductory-Digital-Image-Processing-a-Remote-Sensing-Perspective>
- Jansen LJM, Di-Gregorio A, (2004) Obtaining land-use information from a remotely sensed land cover map: results from a case study in Lebanon. *Int. J. App. Earth Obser. & Geoin.* 5 (2):141-157. <https://doi.org/10.1016/j.jag.2004.02.001>
- Jensen JR, Cowen DC, (1999) Remote sensing of urban/suburban infrastructure and socio-economic attributes. *Photogr. Eng. Remote Sensing* 65:611-622. https://www.asprs.org/wp-content/uploads/pers/99journal/may/1999_may_611-622.pdf
- JiangL, LiuY, WuS, YangC, (2021) Analyzing ecological Environmental change and associated driving factors in China based on NDVI time series data. *Ecol. Indi.*129, 107933. <https://doi.org/10.1016/j.ecolind.2021.107933>
- Kalisa W, Igbawua T, Henchiri M, Ali S, Zhang S, Bai Y, Zhang J, (2019) Assessment of climate impact on vegetation dynamics over East Africa from 1982 to 2015. *Sci. Reports* 9:16865,<https://doi.org/10.1038/s41598-019-53150-0>
- KarnieliA, AgamN, PinkerRT, AndersonM, ImhoffML, GutmanGG, PanovN, GoldbergA, (2010) Use of NDVI and Land Surface Temperature for Drought Assessment: Merits and Limitations. *J. Climate* 23: 618-633. <https://doi.org/10.1175/2009JCLI2900.1>
- KloosS, YuanY, CastelliM, Menzela, (2021) Agricultural Drought Detection with MODIS Based Vegetation Health Indices in Southeast Germany. *Remote Sens.*13, 3907. <https://doi.org/10.3390/rs13193907>
- Liang S, Fang H, Chen M, (2001) Atmospheric Correction of Landsat ETM+ Land Surface Imagery - Part I: Methods. *IEEE Transactions on Geoscience and Remote Sensing* 39(11): 2490-2498. <https://doi.org/10.1109/36.964986>
- LavenderSJ, (2016) Monitoring land cover dynamics at varying spatial scales using high to very high resolution optical imagery. The International Archives of the Photogrammetry, *Remote Sensing and Spatial Informa. Sci.*, Vol. XLI-B8, 23rdISPRS Congress, 12-19 July, Prague, Czech Republic.<https://isprs-archives.copernicus.org/articles/XLI-B8/937/2016/isprs-archives-XLI-B8-937-2016.pdf>
- Lu W, Liu Y, Wang J, Xu W, Wu W, Liu Y, Zhao B, Li H, Li P, (2020) Global proliferation of offshore gas flaring areas. *J. Maps* 16(2): 396-404, DOI: [10.1080/17445647.2020.1762773](https://doi.org/10.1080/17445647.2020.1762773)
- Maaharjan, A. (2018) Land use/land cover of Katrimandu valley by using Remote Sensing and GIS. M.Sc. Dissertation submitted to Central Department of Environmental Sciences, Inst. Sci.& Tech., Tribhuvan Uni., Kirtipur, Kathmandu, Nepal. https://www.academia.edu/37299127/land_use_land_cover_of_kathmandu_valley_by_using_remote_sensing_and_gis
- MolliconeD, AchardF, EvaH, BelwardAS, FedericiS, Lumicisi A, (2003) Land use change monitoring in the Framework of the UNFCCC and its Kyoto Protocol: report on current capabilities of satellite remote sensing technology. European Communities, Luxembourg. EUR, 20867.<https://publications.jrc.ec.europa.eu/repository/handle/JRC26418>

- MorakinyoBO, (2025b) Geospatial Information for Land Use Planning and Sustainable Management. *FUDMA Journal of Sciences (FJS)*9(2): 105-118, DOI: <https://doi.org/10.33003/fjs-2025-0902-3146>
- MorakinyoBO, (2024a) Time Series Analysis from 1984 to 2023 of Earth Observation Satellites Data for Evaluating Changes in Vegetation Cover and Health at Flaring Sites in the Niger Delta, Nigeria. *Academic Platform Journal of Natural Hazards and Disaster Management*5(2): 76-100, DOI: 10.52114/apjhad.1557231
- MorakinyoBO, (2024b) Determination of Mean Sea Level from 1980 TO 2018 Using Tidal Observation Data, Bonny Primary Port, Nigeria. *Science World Journal*19(4): 1176-1184.
- Morakinyo BO, (2024c) Analysis from 1980 TO 2018 of Tidal Observation Data for Assessing the Stability of Tidal Constants for Primary Port. *FUDMA Journal of Sciences (FJS)*8(6): 503-513, DOI: <https://doi.org/10.33003/fjs-2024-0806-3043>
- MorakinyoBO, (2023c) Detection of Impacts of Gas Flaring in the Environment: Application of Landsat Earth Observation Data. *BAZE University J. Entrepreneurship and Interdisciplinary Studies* 2(1): 74-89.<http://dx.doi.org/10.61955/XQBJFP>
- MorakinyoBO, (2023b) Assessments of the impacts of environmental factors on vegetation cover at gas flaring sites in the Niger Delta, Nigeria. *Review of Environ. and Earth Sci.* 10(1): 8-18.<http://dx.doi.org/10.18488/80.v10i1.3390>
- MorakinyoBO, LavenderS, AbbottV, (2023a) Detection of potentially gas flaring related pollution on vegetation cover and its health using remotely sensed data in the Niger Delta, Nigeria. *Asian Review of Environ.& Earth Sci.*10(1): 1-13. <https://doi.org/10.20448/arees.v10i1.4407>
- MorakinyoBO, LavenderS, AbbottV,. (2022b) Evaluation of factors influencing changes in land surface temperature at gas flaring sites in the Niger Delta, Nigeria. *BAZE University J. Entrepreneurship and Interdisciplinary Studies* 1(2): 1-19.<http://dx.doi.org/10.61955/RIIKUF>
- MorakinyoBO, LavenderS, AbbottV, (2022a) Investigation of potential prevailing wind impact on land surface temperature at gas flaring sites in the Niger Delta, Nigeria.*Int. J. Environ. A&ndGeoinfor.* 9(1): 179-190,<https://doi.org/10.30897/ijegeo.968687>
- MorakinyoBO, LavenderS, AbbottV,. (2021) The methodology and results from ground validation of satellite observations at gas Flaring Sites in Nigeria.*Int. J. Environ. and Geoinformatics* 8(3): 290-300, <https://doi.org/10.30897/ijegeo.749664>
- MorakinyoBO, LavenderS, AbbottV, (2020b) Retrieval of land surface temperature from Earth observation satellites for gas flaring sites in the Niger Delta, Nigeria.*Int. J. Environmental Monitoring and Analysis*8(3): 59-74. <https://doi.org/10.11648/j.ijema.20200803.13>
- MorakinyoBO, LavenderS, AbbottV, (2020a) Assessment of uncertainties in the computation of atmospheric correction parameters for Landsat 5 TM and Landsat 7 ETM+ thermal band from atmospheric correction parameter (ATMCORR calculator) *British J. Environ. Sci.*8(1): 20-30. <https://ejournals.org/bjes/vol-8-issue-1-february-2020/assessment-of-uncertainties-in-the-computation-of-atmospheric-correction-parameters-for-landsat-5-tm-and-landsat-7-etm-thermal-band-from-atmospheric-correction-parameter-atmcorr-calculator/>
- MorakinyoBO, LavenderS, SchwarzJ, AbbottV,. (2019) Mapping of land cover and estimation of their emissivity values for gas flaring sites in the Niger Delta. *British J. Environ. Sci.* 7(2): 31-58. <https://www.eajournals.org/wp-content/uploads/Mapping-of-land-cover-and-estimation-of-their-emissivity-values-for-gas-flaring-sites-in-the-Niger-Delta.pdf>
- MorakinyoBO, (2015) Flaring and pollution detection in the Niger Delta using remote sensing. PhD Thesis, University of Plymouth, Plymouth, United Kingdom.<https://dx.doi.org/10.24382/4528>
- Markham BL, Barker JL, (1986) Landsat MSS and TM post-calibration dynamic ranges, exoatmospheric reflectances and at-satellite temperature. EOSAT Landsat Technical Notes: 3-8.<https://www.scirp.org/reference/referencespapers?referenceid=1578935>
- Musa,DG., Oruonye, E. D., Anger, R. T., Ojeh, V. N & Delphine, D. (2024) Effect of Gas Flaring on Human Well-Being and Environ. in Obodo-Ugwa, Ndokwa West, Local Government Area, Delta State, Nigeria. *J. Eng. & Environ. Sci.* 2(1): 000108. <https://medwinpublishers.com/JEESc/effect-of-gas-flaring-on-human-well-being-and-environment-in-obodo-ugwa,-ndokwa-west,-local-government-area,-delta-state,-nigeria.pdf>
- NASA. (2002) National Aeronautics and Space Administration. Landsat 7 ETM+ Science Data Users Handbook.http://www.landsathandbook.gsfc.nasa.gov/data_prod/prog_sect11_3.html [Accessed 23rdJan. 2022].

- NwaoguLA, OnyezeGOC, (2020) Environmental Impacts of Gas Flaring on Ebocha-Egbema, Niger Delta, Nigeria. *Energy & Environ. Res.* **8**(1): 1-11. <https://dergipark.org.tr/tr/pub/apihad/issue/89412/1557231>
- Odukoya OA, (2006) Oil and sustainable development in Nigeria: A case study of the Niger Delta. *Human Ecology* 20(4): 249-258. DOI: [10.31901/24566608.2006/20.04.03](https://doi.org/10.31901/24566608.2006/20.04.03)
- Onosode GO, (2003) Environmental Issues and challenges of the Niger Delta (Perspectives from the Niger Delta Environmental Survey Process) Lagos, Lilybank Property & Trust Limited. https://books.google.com/books/about/Environmental_Issues_and_Challenges_of_t.html?id=MmQ7AQAIAAJ
- Pastor-Guzman, J., Atkinson, P., Dash, J & Rioja-Nieto, R. (2015) Spatio-temporal variation in mangrove chlorophyll concentration using Landsat 8. *Remote Sensing of Environ.* **7**(11): 14530-14558. <http://dx.doi.org/10.3390/rs71114530>
- PettorelliN, VikJO, MysterudA, GaillardJM, TuckerCJ, StensethNC, (2005) Using the satellite-derived NDVI to assess ecological responses to environmental change. *Trends of Ecol.Evol.* **20**(9): 503-510. <https://doi.org/10.1016/J.TREE.2005.05.011>
- Polat AB, Akcay O, Kontas F, (2024) Drought monitoring in Burdur Lake, Turkey using multi-sensor remote sensing data sets. *Ad. Geodesy & Geoinfor. (formerly Geodesy and Cartography)* **73**(1), article no. e47, DOI: [10.24425/agg.2023.146159](https://doi.org/10.24425/agg.2023.146159)
- RoßbergT, SchmittM, (2023) A Globally Applicable Method for NDVI Estimation from Sentinel-1 SAR Backscatter Using a Deep Neural Network and the SEN12TP Dataset. *ISPRS Int. J. Geo-Inf.* **12**: 171-188. <https://doi.org/10.3390/ijgi12040171>
- SanterR, CarrereV, DubuissonP, RogerJC, (1999) Atmospheric correction over land for MERIS. *Int. J. Remote Sens.* **20**: 1819-1840. <https://earth.esa.int/eogateway/documents/20142/37627/MERIS%20ATBD%202015>
- Şatır O, Berberoğlu S, (2012) Land Use/Cover Classification Techniques Using Optical Remotely Sensed Data in Landscape Planning, Landscape Planning, Dr. Murat Ozyavuz (Ed.), ISBN: 978-953-51-0654-8, InTech. [Online]. <http://www.intechopen.com/books/landscape-planning/land-use-cover-classification-techniques-using-optical-remotely-sensed-data-in-landscape-planning> [Accessed 15th May 2023]
- TianJ, WangL, LiX, GongH, ShiC, ZhongR, LiuX, (2017) Comparison of UAV and WorldView-2 imagery for mapping leaf area index of mangrove forest. *Int. J. Appl. Earth Obser. & Geoinfor.* **61**: 22-31. <http://dx.doi.org/10.1016/j.jag.2017.05.002>
- Umbugala,UD&MorakinyoBO, (2023) Detection of Oil and Gas Platforms in the Niger Delta, Nigeria: Role of Digital Technology in Facilities Management. *BAZE University J. Entrep.&Interdis. Stud.* **2**(2): 11-22. <https://boldscholar.com/Home/ArticleLists?volid=21&journalID=12>
- Vicente-Serrano, S. M., Camarero, J. J., Olano, J. M., Martín-Hernández, N., Peña-Gallardo, M., Tomás-BurgueraM, Gazola, Azorin-MolinaC, BhuyanU, El-KenawyA, (2016) Diverse relationships between forest growth and the normalized difference vegetation index at a global scale. *Remote Sens Environ.* **187**: 14-29. <https://doi.org/10.1016/j.rse.2016.10.001>
- Wei W, Zhang H, Zhou J, Zhou L, Xie B, Li C, (2021) Drought monitoring in arid and semi-arid region based on multi-satellite datasets in Northwest China. *Environ Sci & Poll.Res.* **28**: 51556-51574. <https://doi.org/10.1007/s11356-021-14122-y>
- Xiao J, Shen Y, Ge J, Tateishi R, Tang C, Liang Y, Huang Z, (2006) Evaluating urban expansion and land use change in Shijiazhuang, China, by using GIS and remote sensing. *Lands. Urban Plan* **75**(1-2):69-80. <https://doi.org/10.1016/j.landurbplan.2004.12.005>
- Yuan F, Sawaya KE, Loeffelholz BC, Bauer ME, (2005) Land cover classification and change analysis of the Twin Cities (Minnesota) Metropolitan Area by multi-temporal Landsat remote sensing. *Remote Sens. Environ.* **98**(2-3):317-328. <https://doi.org/10.1016/j.rse.2005.08.006>